COMPUTER RESEARCH AND MODELING
2025 VOL. 17 NO. 4 P. 697–715
DOI: 10.20537/2076-7633-2025-17-4-697-715

Ки&М

ANALYSIS AND MODELING OF COMPLEX LIVING SYSTEMS

UDC: 004.94, 577.35

Optimization of proton therapy with radiosensitizing nanoparticles and antiangiogenic therapy via mathematical modeling

M. B. Kuznetsov[a], A. V. Kolobov

P. N. Lebedev Physical Institute of the Russian Academy of Sciences,
53 Leninskiy pr., Moscow, 119991, Russia

E-mail: [a] m.kuznetsov@lebedev.ru

Received 07.07.2025, after completion — 28.07.2025.
Accepted for publication 29.07.2025.

Optimization of antitumor radiotherapy represents an urgent issue, as approximately half of the patients diagnosed with cancer undergo radiotherapy during their treatment. Proton therapy is potentially more efficient than traditional X-ray radiotherapy due to fundamental differences in physics of dose deposition, leading to better targeting of tumors and less collateral damage to healthy tissue. There is increasing interest in the use of non-radioactive radiosensitizing tumor-specific nanoparticles the use of which can boost the performance of proton therapy. Such nanoparticles are small volumes of a sensitizer, such as boron-10 or various metal oxides, enclosed in a polymer layer containing tumor-specific antibodies, which allows for their targeted delivery to malignant cells. Furthermore, a combination of proton therapy with antiangiogenic therapy that normalizes tumor-associated microvasculature may yield further synergistic increase in overall treatment efficacy.

We have developed a spatially distributed mathematical model simulating the growth of a non-invasive tumor undergoing treatment by fractionated proton therapy with nanosensitizers and antiangiogenic therapy. The modeling results suggest that the most effective way to combine these treatment modalities should strongly depend on the tumor cells' proliferation rate and their intrinsic radiosensitivity. Namely, a combination of antiangiogenic therapy with proton therapy, regardless of whether radiosensitizing nanoparticles are used, benefits treatment efficacy of rapidly growing tumors as well as radioresistant tumors with moderate growth rate. In these cases, administration of proton therapy simultaneously with antiangiogenic drugs after the initial single injection of nanosensitizers is the most effective option among those analyzed. Conversely, for slowly growing tumors, maximization of the number of nanosensitizer injections without antiangiogenic therapy proves to be a more efficient option, with enhancement in treatment efficacy growing with the increase of tumor radiosensitivity. However, the results also show that the overall efficacy of proton therapy is likely to increase only modestly with the addition of nanosensitizers and antiangiogenic drugs.

Keywords: mathematical oncology, numerical optimization

Citation: *Computer Research and Modeling*, 2025, vol. 17, no. 4, pp. 697–715.

This work was carried out with the support of the Ministry of Science and Higher Education of the Russian Federation under Agreement 075-15-2025-453 dated 05/30/2025.

КОМПЬЮТЕРНЫЕ ИССЛЕДОВАНИЯ
И МОДЕЛИРОВАНИЕ 2025 Т. 17 № 4 С. 697–715
DOI: 10.20537/2076-7633-2025-17-4-697-715

Ки&М

АНАЛИЗ И МОДЕЛИРОВАНИЕ СЛОЖНЫХ ЖИВЫХ СИСТЕМ

УДК: 004.94, 577.35

Оптимизация протонной терапии с радиосенсибилизирующими наночастицами и антиангиогенной терапии с помощью математического моделирования

М. Б. Кузнецов[a], А. В. Колобов

Физический институт имени П. Н. Лебедева Российской академии наук,
Россия, 119991, г. Москва, Ленинский проспект, д. 53

E-mail: [a] m.kuznetsov@lebedev.ru

Получено 07.07.2025, после доработки — 28.07.2025.
Принято к публикации 29.07.2025.

Оптимизация противоопухолевой радиотерапии является актуальной проблемой, поскольку примерно половина пациентов с диагнозом рак проходят радиотерапию во время лечения. Протонная терапия потенциально более эффективна, чем традиционная фотонная терапия из-за фундаментальных различий в физике распределения дозы, которые приводит к лучшему нацеливанию на опухоли и меньшему сопутствующему повреждению здоровых тканей. В настоящее время наблюдается растущий интерес к использованию нерадиоактивных радиосенсибилизирующих опухолеспецифических наночастиц, использование которых может повысить эффективность протонной терапии. Такие наночастицы представляют собой небольшие объемы сенсибилизатора, например, бора-10 или различных оксидов металлов, заключенных в полимерный слой, содержащий опухолеспецифические антитела, что позволяет осуществлять их направленную доставку к злокачественным клеткам. Кроме того, сочетание протонной терапии с антиангиогенной терапией, которая нормализует микрососудистую сеть, связанную с опухолью, может дать дальнейшее синергетическое увеличение общей эффективности лечения.

Мы разработали пространственно распределенную математическую модель, имитирующую рост неинвазивной опухоли, проходящей лечение фракционированной протонной терапией с наносенсибилизаторами и антиангиогенной терапией. Результаты моделирования показывают, что наиболее эффективный способ комбинирования этих методов лечения должен существенно зависеть от скорости пролиферации опухолевых клеток и их собственной радиочувствительности. А именно, сочетание антиангиогенной терапии с протонной терапией, независимо от того, используются ли радиосенсибилизирующие наночастицы, должно повысить эффективность лечения быстрорастущих опухолей, а также радиорезистентных опухолей с умеренной скоростью роста. В этих случаях применение протонной терапии одновременно с антиангиогенными препаратами после первоначальной однократной инъекции наносенсибилизаторов является наиболее эффективным вариантом лечения среди проанализированных. Напротив, для медленнорастущих опухолей максимизация количества инъекций наносенсибилизаторов без антиангиогенной терапии оказывается более эффективным вариантом, причем повышение эффективности лечения растет с ростом радиочувствительности опухоли. Однако результаты также показывают, что общая эффективность протонной терапии, вероятно, должна увеличиться лишь умеренно при добавлении наносенсибилизаторов и антиангиогенных препаратов.

Ключевые слова: математическая онкология, численная оптимизация

Работа выполнена при поддержке Министерства науки и высшего образования РФ в рамках Соглашения 075-15-2025-453 от 30.05.2025.

Introduction

Compared to traditional X-ray radiation therapy, proton therapy represents a potentially more effective modality, as it allows targeting tumors more precisely, while minimizing exposure to surrounding healthy tissues. This is due to the unique physical properties of charged particles, specifically the deposition of a substantial fraction of their energy at a certain depth in tissue [Brown, Suit, 2004]. This feature makes proton therapy particularly beneficial for treating tumors near critical structures (like the brain, spine, or eyes) or in pediatric patients, whose developing tissues are more sensitive to radiation. Currently, there are over a hundred proton therapy centers worldwide, with proton therapy rapidly becoming more widespread as the relevant technologies advance [Tsang, Timmerman, 2004].

There is growing interest in using nonradioactive elements during proton therapy for improved imaging [Galanakou et al., 2022] and for improved tumor radiosensitization [Azarkin et al., 2023; Hu et al., 2024; Bilynsky et al., 2022]. Generally, small volumes of a sensitizer, e. g., boron-10 or different metal oxides, are encased in a polymer layer that contains tumor-specific antibodies to enable targeted delivery to malignant cells. The mechanisms by which sensitizers enhance proton therapy include physical dose enhancement through secondary electron emission, catalytic generation of reactive oxygen species, and nuclear reactions with protons [Azarkin et al., 2023; Chuang et al., 2023]. Clinical translation of nanosensitizers for proton therapy is still in its early stages. A few nanoparticle formulations have entered clinical trials, but further research is required for estimating long-term safety and efficacy [Hu et al., 2024; Hu et al., 2023]. Current challenges include optimizing nanoparticle design, improving tumor targeting and uptake, and better understanding of the biological mechanisms of radiosensitization. Our research group has conducted studies on nanoparticle-enhanced proton therapy for cancer treatment, focusing on the use of boron and bismuth nanoparticles, which showed excellent potential as sensitizers, significantly enhancing cancer cell death [Zavestovskaya et al., 2023; Popov et al., 2024; Zavestovskaya et al., 2024].

An increase in treatment efficacy can be achieved not only by introdicing novel technologies into clinical practice but also by rationalization of the use of already implemented modalities. A combination of different therapies can yield synergistic increase in overall treatment efficacy. In that light, combination of radiotherapy with antiangiogenic therapy represents an intriguing option. Angiogenesis, i. e., formation of new blood vessels, is a major factor in tumor development and progression, crucial for increase of blood supply to the tumor to meet its increased metabolic needs [Hanahan, Weinberg, 2000]. Antiangiogenic therapy leads to normalization of tumor-associated capillaries and to cessation of their further formation, restricting tumor nutrient supply [Gee et al., 2003]. Antiangiogenic therapy by itself can delay tumor growth but mostly do not cause tumor regression [Jayson et al., 2016]. Interestingly, due to vessel normalization, antiangiogenic therapy can lead to transient increase in tumor oxygenation which can enhance the effects of radiotherapy, since oxygen represents a prominent radiosensitizer [Jain, 2005].

There is growing interest in combining radiotherapy with antiangiogenic therapy. Some studies have shown promising results combining antiangiogenic drugs like bevacizumab with radiotherapy for various cancers, however, larger clinical trials have reported variable efficacy and increased toxicity with the combination [Goedegebuure et al., 2019]. Optimizing the combination regimens to maximize efficacy while minimizing toxicity is an ongoing focus [Goedegebuure et al., 2019; Bendavid, Modesto, 2022], with more research needed on proton therapy specifically, as most studies have used conventional photon radiotherapy.

Combined use of antiangiogenic therapy and proton radiotherapy with the use of radiosensitizing nanoparticles is a double-edge sword, since in long-term antiangiogenic effects lead to decrease of penetration of nanoparticles in tumor, as well as to decreased tumor oxygenation and proliferation

activity, which contributes to decreased tumor cell radiosensitivity. The choice of proper protocol of combined therapy can increase treatment efficacy, but this task is complicated by significant inter-patient variability. Potential optimal protocols should largely vary for different patients, while the possibility of measuring patient-specific parameters in clinical setting is significantly limited. Mechanistic mathematical modeling offers a valuable tool to address these challenges and facilitate treatment optimization.

In current context, mechanistic modeling involves representing biological objects via equations which terms correspond to specific natural laws. Mechanistic modeling in oncology is gaining momentum, having led to at least six prospective clinical trials testing optimized scheduling of chemotherapeutic and targeted drugs [McDonald et al., 2023], and to three trials exploring optimization of external beam radiotherapy — NCT03557372 [Leder et al., 2014], NCT03656133 [López et al., 2018], and NCT03768856 [Prokopiou et al., 2015].

Nowadays, for the study of proton therapy with nanosensitizers, different mathematical modeling techniques are used for calculating dose distributions, predicting nanoparticle uptake by cells, and estimating dose enhancement ratios [Song et al., 2023; Cunningham et al., 2021]. However, the simulations of a whole-course of proton therapy with nanosensitizers via mechanistic modeling are rare. To the best of our knowledge, previously we were the first to perform the relative simulations, suggesting that spatial optimization of irradiation can increase tumor cell damage for each irradiation, while faster suppression of angiogenesis may represent an efficient way towards minimization of tumor cell repopulation [Kuznetsov, Kolobov, 2023a]. In another work we showed that the optimal size of nanosensitizers for achieving maximum tumor radiosensitization crucially depends on the permeability of tumor capillaries [Kuznetsov, Kolobov, 2023c]. The current study on optimization of proton radiotherapy with radiosensitizing nanoparticles and antiangiogenic therapy is based on these and others of our previous works on optimization of external beam radiotherapy [Kuznetsov, Kolobov, 2020; Kuznetsov, Kolobov, 2023b; Kuznetsov, Kolobov, 2022; Kuznetsov et al., 2018].

Mathematical model

Equations

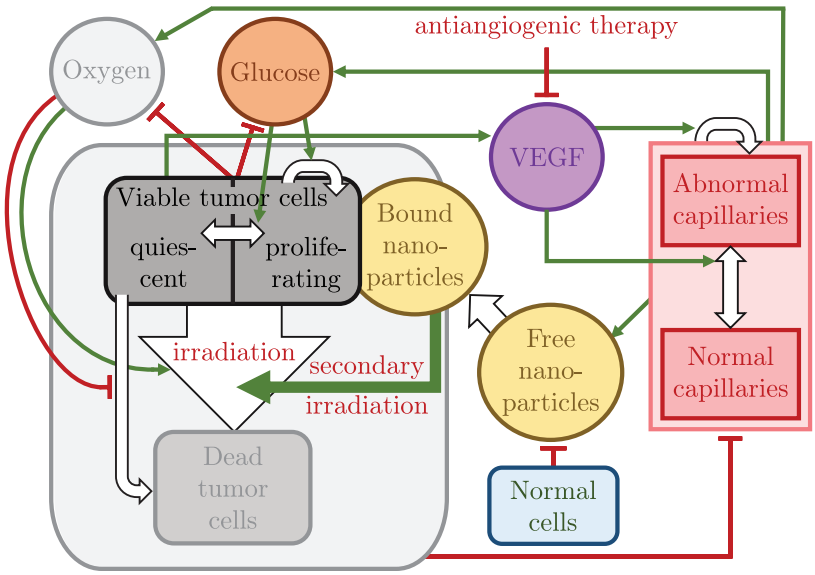

Figure 1. Scheme of the main model interactions governed by Eqs. (1). Green arrows denote stimulating interactions, red lines show inhibiting interactions, white arrows mark transitions of variables

The used mathematical model contains eleven variables, which are the functions of spatial and temporal coordinates r and t. One non-spatially-distributed variable corresponds to the concentration of nanosensitizers in the bloodstream. Injections of nanosensitizers, performing of spatially uniform irradiations, and antiangiogenic treatment via elimination of proangiogenic factors represent the external controls of the otherwise autonomous system of Eqs. (1). The block scheme of the main model interactions is shown in Fig. 1.

$$
\begin{aligned}
&\text{proliferating tumor cells:} && \frac{\partial n_p}{\partial t} = \overbrace{Bn_p\frac{g}{g+g^*}}^{\text{proliferation}} \overbrace{-B\cdot[1-\Theta_{tr}(g)]n_p + B\cdot\Theta_{tr}(g)n_q}^{\text{transition}} \overbrace{-R_p}^{\text{irradiation}} \overbrace{-\frac{1}{r^2}\frac{\partial\left(In_pr^2\right)}{\partial r}}^{\text{convection}};\\
&\text{quiescent tumor cells:} && \frac{\partial n_q}{\partial t} = \overbrace{B\cdot[1-\Theta_{tr}(g)]n_p - B\cdot\Theta_{tr}(g)n_q}^{\text{transition}} \overbrace{-\Phi(w)n_q}^{\text{starvation}} \overbrace{-R_q}^{\text{irradiation}} \overbrace{-\frac{1}{r^2}\frac{\partial\left(In_qr^2\right)}{\partial r}}^{\text{convection}};\\
&\text{normal cells:} && \frac{\partial h}{\partial t} = \overbrace{-\frac{1}{r^2}\frac{\partial\left(Ihr^2\right)}{\partial r}}^{\text{convection}};\\
&\text{dead cells:} && \frac{\partial m}{\partial t} = \overbrace{R_p+R_q}^{\text{irradiation}} \overbrace{+\Phi(w)n_q}^{\text{starvation}} \overbrace{-Mm}^{\text{outflow}} \overbrace{-\frac{1}{r^2}\frac{\partial\left(Imr^2\right)}{\partial r}}^{\text{convection}};\\
&\text{VEGF:} && \frac{\partial v}{\partial t} = \overbrace{S_vn_q}^{\text{secretion}} \overbrace{-\xi[c_n+c_a]v}^{\text{internalization}} \overbrace{-M_vv}^{\text{degradation}} \overbrace{+D_v\Delta v}^{\text{diffusion}};\\
&\text{normal capillaries:} && \frac{\partial c_n}{\partial t} = \overbrace{-M_c[n_q+m]c_n}^{\text{degradation}} \overbrace{+\frac{V_nv^*}{v+v^*}c_a}^{\text{normalization}} \overbrace{-\frac{V_dv}{v+v^*}c_n}^{\text{denormalization}} \overbrace{-\mu[c_n-1]}^{\text{recovery}};\\
&\text{abnormal capillaries:} && \frac{\partial c_a}{\partial t} = \overbrace{-M_c[n_p+n_q+m]c_a}^{\text{degradation}} \overbrace{+\frac{Rv}{v+v^*}[c_n+c_a]\left[1-\frac{c_n+c_a}{c_{\max}}\right]}^{\text{angiogenesis}} \overbrace{-\frac{V_nv^*}{v+v^*}c_a}^{\text{normalization}} \overbrace{+\frac{V_dv}{v+v^*}c_n}^{\text{denormalization}} \overbrace{+\frac{D_c}{r^2}\frac{\partial^2\left(gr^2\right)}{\partial r^2}}^{\text{active motion}};\\
&\text{glucose:} && \frac{\partial g}{\partial t} = \overbrace{\left[P_n^gc_n+P_a^gc_a\right]\cdot[1-g]}^{\text{inflow}} \overbrace{-\left[\{\nu_gB\}n_p+Q_h^g\{n_q+h\}\right]\frac{g}{g+g^*}}^{\text{consumption}} \overbrace{+\frac{D_g}{r^2}\frac{\partial^2\left(gr^2\right)}{\partial r^2}}^{\text{diffusion}};\\
&\text{oxygen:} && \frac{\partial w}{\partial t} = \overbrace{P_w(c_n,\,c_a)[S(w_A)-S(w)]}^{\text{inflow}} \overbrace{-\left[\{\nu_wB\}n_p+Q_h^g\{n_q+h\}\right]\frac{w}{w+w^*}}^{\text{consumption}} \overbrace{+\frac{D_w}{r^2}\frac{\partial^2\left(wr^2\right)}{\partial r^2}}^{\text{diffusion}};\\
&\text{free nanoparticles:} && \frac{\partial u_f}{\partial t} = \overbrace{\left[P_n^uc_n+P_a^uc_a\right]\cdot[u-u_f]}^{\text{inflow/outflow}} \overbrace{-\kappa[n_p+n_q]u_f}^{\text{binding}} \overbrace{-N_f}^{\text{reaction}} \overbrace{+\frac{D_u}{r^2}\frac{\partial^2\left(u_fr^2\right)}{\partial r^2}}^{\text{diffusion}};\\
&\text{bound nanoparticles:} && \frac{\partial u_b}{\partial t} = \overbrace{\kappa[n_p+n_q]u_f}^{\text{binding}} \overbrace{-N_b}^{\text{reaction}} \overbrace{-Mmu_b}^{\text{outflow}} \overbrace{-\frac{1}{r^2}\frac{\partial\left(Iu_br^2\right)}{\partial r}}^{\text{convection}};\\
&\text{nanoparticles in blood:} && \frac{\partial u}{\partial t} = \overbrace{\sum_{i=1}^{F}\delta(t-t_i)}^{\text{injections}} \overbrace{-Cu}^{\text{clearance}};\\
&\text{irradiations:} && R_x \equiv R_x(r,\,t) = \Gamma_x(u_b(r,\,t))\cdot\left[\sum_{j=1}^{F}\delta(t-t_j)\right]\cdot n_x(r,\,t), \quad x = p,\,q;
\end{aligned}
\tag{1}
$$

$$\text{where } n_p + n_q + h + m = 1,$$

$$\Phi(w) = \begin{cases} 0 \text{ if } w \geqslant w^*; \\ M\left[\left\{\frac{w}{w^*}\right\}^2 - 2\frac{w}{w^*} + 1\right] \text{ if } w < w^*; \end{cases}$$

$$P_w(c_n, c_a) = P_w^0 \cdot \frac{1.5[c_n + c_a]}{0.5 + c_n + c_a}; \quad S(w) = \frac{w^\chi}{w^\chi + \widehat{w^\chi}};$$

$$\Gamma_x(u_b(r, t)) = 1 - \exp\left(-k_x\left\{\alpha \cdot D(t) \cdot [OER_\alpha(w(r, t)) + K_u \cdot \{N_b(r, t) + N_f(r, t)\}] + \right.\right.$$
$$\left.\left. + \beta[D(t) \cdot OER_\beta(w(r, t))]^2\right\}\right), \quad x = p, q;$$

$$N_y \equiv N_y(r, t) = \left[1 - e^{-\alpha_{NP} \cdot D(t)}\right] \cdot \left[\sum_{j=1}^{F} \delta(t - t_j)\right] \cdot u_y(r, t), \quad y = f, b;$$

$$OER_y(w) = \frac{w \cdot OER_y^{\max} + K_m}{w + K_m}, \quad y = \alpha, \beta.$$

The model describes spherically symmetric growth of a non-invasive tumor within normal tissue. When supplied with adequate glucose g and oxygen w, tumor cells exist in a proliferative state n_p, with the rate of cell proliferation depending on the rate at which they consume glucose. Glucose is considered explicitly in the model, since it is an indispensable substrate for biosynthesis of several types of molecules, without which cell division is impossible [Patra, Hay, 2014]. In the absence of glucose, cells reversibly transit to a quiescent state n_q. Following irradiation, some of the proliferating and quiescent cells move to the dead state m. Dead cells are gradually eliminated from the simulation region. For simplicity, we neglect the possibility of tumor cell senescence after irradiation. Therefore, the alive tumor cells remaining after the therapy in the model represent the clonogenic malignant cells, which can give rise to tumor recurrence. Minimization of the number of alive tumor cells will further represent the main goal of treatment optimization. Tumor cells are surrounded by normal cells h, with the tumor and normal tissues assumed to be saturated and incompressible, meaning that the total density of cells remains constant and normalized to unity.

Two types of capillaries are considered: normal c_n and abnormal c_a. The latter exhibit increased permeability to glucose and nanoparticles due to the influence of vascular endothelial growth factor (VEGF) v. VEGF not only promotes increased capillary permeability but also stimulates angiogenesis, leading to the formation of new capillaries in abnormal state. VEGF is produced by nutrient-deprived quiescent cells and is distributed through tissue by diffusion. At low VEGF concentrations, the capillaries return to normal state. Additionally, blood capillaries within the tumor degrade due to rupture, which is implicitly assumed to be caused by mechanical displacement and chemical factors [Holash et al., 1999].

Glucose and oxygen flow from the capillaries into the tissue, diffuse through it, and are utilized by the cells. Proliferating tumor cells consume these resources at a significantly faster rate than quiescent tumor cells and normal cells. For a more detailed explanation of these aspects of the model, we refer the readers to our previous work [Kuznetsov, Kolobov, 2023c] and to our study [Kuznetsov, Kolobov, 2018], where we introduced the method for simulating oxygen dynamics.

The damage to tumor cells from irradiation is modeled using a modified version of the standard linear-quadratic equation, which estimates the number of cells surviving after a single dose of irradiation D [Joiner, van der Kogel, 2018]. The modifications consider three factors that influence tumor cell radiosensitivity. The first is the oxygen effect, which indicates that oxygenated cells are significantly more radiosensitive than hypoxic cells. The second factor is the increased radiosensitivity of proliferating cells compared to quiescent cells. These factors are incorporated in the manner described in our previous work [Kuznetsov, Kolobov, 2020]. The third factor, introduced in our studies [Kuznetsov, Kolobov, 2023a; Kuznetsov, Kolobov, 2023c], is the effective increase of cell

radiosensitivity via the additional dose delivered in a series of reactions involving sensitizers associated with nanoparticles near tumor cells. This effect is assumed to influence only the linear component of tumor cell radiosensitivity and to operate independently of the oxygen effect.

The nanoparticles enter the tissue from the bloodstream through diffusion via the pores in capillary walls. Convective flow of nanoparticles is not considered in this model, as a not significant aspect in the absence of variation of relative parameters influencing it, while its omission allows one to drastically speed up the calculations. Once in the tissue, nanoparticles exist in a free state u_f and diffuse passively. Nanoparticles are cleared through capillaries back into the bloodstream unless they specifically bind to tumor cells. In the bound state u_b, they become immobilized relative to the tumor cells. Upon irradiation, both free and bound nanosensitizers contribute to increasing the effective dose delivered to cells.

The treatment starts when tumor radius R^T achieves 5 mm. Time-dependent variable representing the concentration of nanoparticles in the blood, $u(t)$, increases instantaneously at designated time points, t_i. Irradiation is applied instantaneously at specific time points, t_j, occurring F times during the treatment. In this study, we consider a standard temporal fractionation of radiotherapy, involving 30 irradiations administered on weekdays over six consecutive weeks. The dose used for irradiations is fixed as $D = 1.8$ Gy, which is typical for proton therapy delivered in this manner. The action of antiangiogenic therapy is modeled as having the maximum theoretically possible efficacy. Upon the start of treatment, it is assumed that all existing VEGF immediately binds to the antiangiogenic drug, thereby neutralizing it. However, the normalization of the microvasculature does not occur instantaneously. The dynamics of the accompanying processes unfold at physiologically relevant rates. We vary both the timing of nanosensitizer injections and the time of onset of antiangiogenic therapy to identify more effective treatment strategies.

Parameters

The model includes several dozen parameters, which were estimated based on the results from various experiments or calibrated to reflect the known general characteristics of tumor growth when direct estimation was not feasible. The basic set of parameters is presented in Table 1, where the following normalization parameters were used to derive their model values: 1 h for time; 10^{-2} cm for length; $3 \cdot 10^8$ cells/mL for cell density; $v = 10^{-11}$ mol/mL for VEGF concentration; 100 cm^2/cm^3 for capillary surface area density; 1 mg/mL for glucose concentration; 11 mM for oxygen concentration; and 1 Gy for irradiation dose. The normalization factor for nanoparticle concentration is not explicitly used, as it is linearly related to the factor of dose enhancement by nanoparticles, K_u. The maximum rate of tumor cell proliferation B and the value of tumor cells linear radiosensitivity α are varied in this study in order to investigate their influence on the treatment outcome and on the optimal therapy approach.

The selection of most of these model parameters is explained in our work [Kuznetsov, Kolobov, 2023c]. The ratio of tumor cell radiosensitivity parameters $\frac{\alpha}{\beta}$ is typical for many tumor cell lines [Joiner, van der Kogel, 2018]. The expenditure of the radiosensitizer during irradiation is configured to approach saturation at the dose D. The dose enhancement factor due to sensitizer, K_u, is calibrated based on findings from our experimental group, which indicate that the use of nanosensitizers can lead to an effective dose increase of approximately 30 % under well-oxygenated conditions. The parameters governing the diffusion and penetration of nanoparticles from the capillaries are based on nanoparticles with a 13 nm radius, which was identified in our work [Kuznetsov, Kolobov, 2023c] as being near optimal for achieving maximum tumor radiosensitization. The increased permeability of abnormal capillaries allows us to replicate the well-known phenomenon of enhanced permeability and retention associated with high molecular weight substances in tumors [Wu, 2021].

Table 1. Model parameters

Parameter	Description	Value	Based on
Cells:			
B	maximum rate of tumor cell proliferation	0.01–0.04	[Freyer, Sutherland, 1985]
ϵ	smoothing parameter of Heaviside function	500	[Kuznetsov, Kolobov, 2023c]
M	maximum rate of outflow of dead tumor cells	0.001	[Kuznetsov, Kolobov, 2023c]
VEGF:			
S_v	secretion rate	1	[Kelm et al., 2005]
ξ	internalization rate	1	[Mac Gabhann, Popel, 2007]
M_v	degradation rate	0.01	[Köhn-Luque et al., 2013]
D_v	diffusion coefficient	21	[Köhn-Luque et al., 2013]
Capillaries:			
R	maximum rate of angiogenesis	0.01	[Dickson et al., 2007]
$c_{\max}$	maximum surface area density	5	[Dickson et al., 2007]
M_c	degradation rate	0.05	[Stamatelos et al., 2014]
V_n	normalization rate	0.1	[Dings et al., 2007]
V_d	denormalization rate	0.1	[Dings et al., 2007]
μ	recovery rate	0.002	[Kuznetsov, Kolobov, 2018]
v^*	Michaelis constant for VEGF action	0.001	[Kuznetsov, Kolobov, 2023c]
D_c	coefficient of active motion	0.03	[Stamatelos et al., 2014]
Glucose:			
g^*	Michaelis constant for consumption	0.01	[Casciari et al., 1992]
P_n^g	permeability of normal capillaries	4	[Clough, Smaje, 1984]
P_a^g	permeability of abnormal capillaries	10	[Kuznetsov, Kolobov, 2018]
ν_g	coefficient of proliferating tumor cells consumption rate	1200	[Freyer, Sutherland, 1985]
Q_h^g	rate of consumption by normal cells	0.5	[Baker, Mottram, 1973]
D_g	diffusion coefficient	100	[Tuchin et al., 2001]
Oxygen:			
w^*	Michaelis constant for consumption rate	0.005	[Casciari et al., 1992]
P_w^0	inflow parameter	50	[Richardson et al., 2006]
w_A	oxygen concentration in artery	5.87	[Pittman, van der Kogel, 2011]
$\widehat{w}$	concentration at which hemoglobin saturation is 50 %	1.56	[Clerbaux et al., 1993]
χ	Hill coefficient for oxygen-hemoglobin dissociation curve	2.55	[Clerbaux et al., 1993]
Q_n^w	coefficient of proliferating tumor cells consumption rate	6400	[Freyer, Sutherland, 1985]
Q_h^w	consumption rate by normal tissue	8	[Baker, Mottram, 1973]
D_w	diffusion coefficient	720	[Androjna et al., 2008]
Irradiation:			
α	linear parameter of tumor cell radiosensitivity	0.05–0.4	see text
β	quadratic parameter of tumor cell radiosensitivity	$10 \cdot \alpha$	[Joiner, van der Kogel, 2018], see text
D	irradiation dose	1.8	see text
$OER_\alpha^{\max}$	maximum OER_α under aerobic conditions	2.4	[Iwata et al., 2016]
$OER_\beta^{\max}$	maximum OER_β under aerobic conditions	2.7	[Iwata et al., 2016]
K_m	Michaelis constant for oxygen enhancement effect	0.193	[Wouters, Brown, 1997]
k_p	coefficient of radiosensivity of proliferating cells	1	[Zhao et al., 2017]
k_q	coefficient of radiosensivity of quiescent cells	0.2	[Zhao et al., 2017]
K_u	factor of dose enhancement by nanosensitizers	5	see text
Nanoparticles:			
κ	coefficient of binding with tumor cells	0.5	[Kuznetsov, Kolobov, 2023c]
D_u	diffusion coefficient	5	[Kuznetsov, Kolobov, 2023c]
C_u	clearance rate	0.09	[Zelepukin et al., 2019]
P_n^u	permeability of normal capillaries	0.001	[Kuznetsov, Kolobov, 2023c]
P_a^u	permeability of abnormal capillaries	0.18	[Kuznetsov, Kolobov, 2023c]
α_{NP}	coefficient of sensitizer expenditure	2	see text

Numerical solving

The computational code was implemented in C++. During the numerical simulation of Eqs. (1), the equation for dead cells was not considered explicitly due to the conservation law $m = 1 - n_p - n_q - h$. Equations for glucose and oxygen were considered in the quasistationary approximation due to the fast dynamics of these variables and were solved using the tridiagonal matrix algorithm. For other variables, the kinetic, diffusion, and convection equations were solved sequentially at each time step. The kinetic equations were solved using the explicit Euler method, which is justified by the relatively small used time steps. For the diffusion equations, the implicit Crank–Nicholson scheme was employed. These classical methods are detailed, e. g., in the book [Press, 2007]. The convective equations were solved using the conservative method, previously introduced by us in the work [Kuznetsov, Kolobov, 2023b], which introduces two floating grid points on the otherwise uniform grid to explicitly maintain the sharp edge of normal tissue and the distinct boundary between tumor and normal tissue, which should exist due to the absence of intrinsic motility of tumor cells. This feature enables precise measurements of the tumor radius $R^T(t)$ and normal tissue radius $R^N(t)$.

The following initial conditions were used, representing a spherical section of normal tissue of initial radius $R_0^N = 10$ mm with a small spherical colony of tumor cells of radius $R_0^T = 0.2$ mm located in its center, where concentration of glucose and oxygen follow their quasistationary distributions:

$$\begin{cases} n_p(r,\,0) = 1, \\ h(r,\,0) = 0, \\ g(r,\,0) = g_{st}(r,\,0), \\ w(r,\,0) = w_{st}(r,\,0), \\ c_n(r,\,0) = 0, \\ n_q(r,\,0) = 0, \\ v(r,\,0) = 0, \\ c_a(r,\,0) = 0, \\ u_f(r,\,0) = 0, \\ u_b(r,\,0) = 0 \end{cases} \text{for } r \leqslant R_0^T; \qquad \begin{cases} n_p(r,\,0) = 0, \\ h(r,\,0) = 1, \\ g(r,\,0) = g_{st}(r,\,0), \\ w(r,\,0) = w_{st}(r,\,0), \\ c_n(r,\,0) = 1, \\ n_q(r,\,0) = 0, \\ v(r,\,0) = 0, \\ c_a(r,\,0) = 0, \\ u_f(r,\,0) = 0, \\ u_b(r,\,0) = 0 \end{cases} \text{for } R_0^T < r \leqslant R_0^N. \tag{2}$$

The following boundary conditions were used:

$$\begin{gathered} \forall t \quad \left.\frac{\partial n_p}{\partial r}\right|_0 = \left.\frac{\partial n_q}{\partial r}\right|_0 = \left.\frac{\partial h}{\partial r}\right|_{R_0^T} = \left.\frac{\partial v}{\partial r}\right|_0 = \left.\frac{\partial c_n}{\partial r}\right|_0 = \left.\frac{\partial c_a}{\partial r}\right|_0 = \left.\frac{\partial g}{\partial r}\right|_0 = \left.\frac{\partial w}{\partial r}\right|_0 = \left.\frac{\partial u_f}{\partial r}\right|_0 = \left.\frac{\partial u_b}{\partial r}\right|_0 = 0; \\ \left.\frac{\partial n_p}{\partial r}\right|_{R^T} = \left.\frac{\partial n_q}{\partial r}\right|_{R^T} = \left.\frac{\partial h}{\partial r}\right|_{R^N} = \left.\frac{\partial v}{\partial r}\right|_{R^N} = \left.\frac{\partial g}{\partial r}\right|_{R^N} = \left.\frac{\partial w}{\partial r}\right|_{R^N} = \left.\frac{\partial u_f}{\partial r}\right|_{R^N} = \left.\frac{\partial u_b}{\partial r}\right|_{R^N} = 0; \\ c_a\left(R^N,\,t\right), \quad c_n\left(R^N,\,t\right) = 1. \end{gathered} \tag{3}$$

During the numerical solution, the convective motion field $I(r,\,t)$ for the cells and bound nanoparticles was calculated by the following equation, obtained by summing the dynamic equations of all cells in Eqs. (1) and setting the convective flow velocity to zero at $r = 0$:

$$I(r,\,t) = \frac{1}{r^2}\int\limits_0^r \left\{ Bn_p(z,\,t)\frac{g(z,\,t)}{g(z,\,t) + g^*} - Mm(z,\,t) \right\} z^2\,dz. \tag{4}$$

Results

Tumor profiles under different treatments

Figure 2, *a* illustrates the initial distributions of model variables. At the beginning of tumor growth, the tumor consists entirely of proliferating cells, whose number grows almost exponentially. However, shortly some tumor cells begin to experience deficiency of glucose supplied by normal capillaries. Therefore, tumor cells begin transitioning into quiescent state and secreting proangiogenic factor VEGF. As Fig. 2, *b* shows, this results in formation of abnormal capillaries, concentrated predominately in the normal tissue close to the tumor rim. Along with the degradation of capillaries inside the tumor, this results in a layered tumor structure, with the inner core primarily composed of quiescent cells and the outer rim consisting of proliferating cells. This structure is characteristic of tumor spheroids in experimental settings and non-invasive tumors in vivo [Stamatelos et al., 2014]. Although glucose levels elevate in the peritumoral region due to the increased permeability and density of abnormal capillaries, microvasculature modified by angiogenesis can support only a fraction of tumor cells in the proliferative state.

In 87 days, the tumor reaches the radius of $R^T = 5$ mm, which marks the beginning of treatment, three types of which are illustrated. At this moment, nanoparticles can be injected in the bloodstream, with Fig. 2, *c* corresponding to one day after their injection. A portion of nanoparticles binds to tumor cells, predominantly in the tumor rim, located close to abnormal capillaries. Figures 2, *d*, *e* show the outcomes of a single irradiation at the second day of treatment with and without preliminary nanoparticles injection. In both cases, the resulting distribution of dead tumor cells illustrates the heterogeneity in tumor cell radiosensitivity. Deep within the tumor, the cells remain in a hypoxic non-proliferative state, with only a moderate fraction of them dying. In contrast, near the tumor rim, most of the cells transit into dead state. However, the presence of nanoparticles increases the fraction of dead cells from $\approx 11\,\%$ to $\approx 14\,\%$ in the tumor core, and from $\approx 70\,\%$ to $\approx 99.97\,\%$ in the tumor rim. More active death of tumor cells bound to nanoparticles leads to decreased overall consumption of nutrients by tumor, evidenced by notably elevated oxygen pressure at the tumor-normal tissue interface, as well as by deeper penetration of oxygen and glucose into the tumor. Since nanoparticles are cleared out of the body rapidly, their penetration into the tumor significantly declines within several days, and their contribution to the efficacy of the following irradiations becomes minor.

Figure 2, *f* corresponds to another distribution of variables on the second day of treatment, but with antiangiogenic therapy having been performed simultaneously with the first irradiation, after the injection of nanoparticles. Up to this moment, antiangiogenic therapy does not influence the tumor cells distribution to any notable extent, but elimination of VEGF leads to ongoing normalization of capillaries that surround the tumor. As Figs. 2, *g*, *h* show, after more than a month antiangiogenic therapy does lead to prominent normalization of capillary density, however, such normalization happens in the absence of antiangiogenic therapy as well, although to a smaller extent. The reason for that is notable efficacy of irradiations for the considered parameter set, eventually leading to elimination of the vast majority of tumor cells, halting of VEGF production, and elevation of nutrient levels inside the shrunk tumors close to their levels in normal tissue. Nevertheless, antiangiogenic therapy does lead to an increase of overall treatment efficacy in the considered simulations. While mono-radiotherapy leads to a minimal number of alive tumor cells $N \approx 16$ and the injection of nanoparticles allows decreasing this number to $N \approx 7$, addition of antiangiogenic therapy yields further decrease of this parameter down to $N \approx 4$. This parameter is calculated as

$$N = \min_t \int_0^{R^T} [n_p + n_q] r^2 \, dr.$$

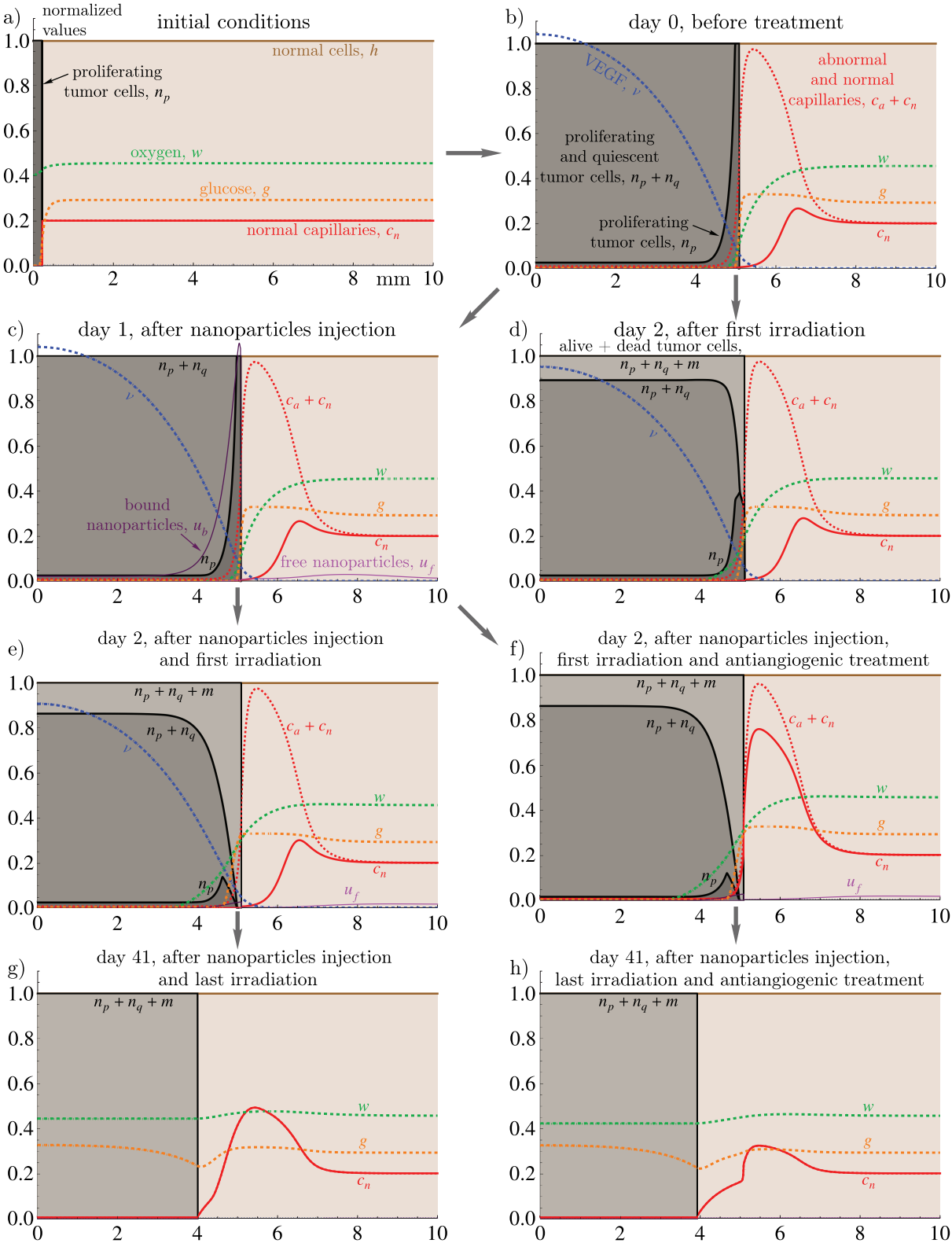

Figure 2. Distributions of model variables obtained by numerical simulations of Eqs. (1) with initial conditions (2) and boundary conditions (3). The maximum rate of tumor cell proliferation $B = 0.02$, tumor cell radiosensitivity $\alpha = 0.25$, the values of other parameters are given in Table 1

In terms of tumor cure probability (TCP), which is traditionally calculated by the formula $TCP(N) = e^{-N}$ [Munro, Gilbert, 1961], these cell numbers correspond to $TCP \approx 0\,\%$, $\approx 0.1\,\%$, and $\approx 1.6\,\%$. This finding, however, does not guarantee that such addition of antiangiogenic therapy will be beneficial for any physiologically reasonable values of model parameters, and the relevant investigation is performed below.

Efficacy of radiotherapy depending on tumor cell radiosensitivity and proliferation rate

In this study we perform a variation of two parameters: tumor cell radiosensitivity and maximum tumor cell proliferation rate as they have been identified by us previously to be the major parameter influencing the outcome of radiotherapy in mono-regime [Kuznetsov, Kolobov, 2023b] and in combination with antiangiogenic therapy [Kuznetsov et al., 2018]. At first, let's consider the influence of these parameters on the outcome of mono-radiotherapy, as well involving 30 irradiations administered on weekdays over six consecutive weeks.

As Fig. 3 shows, expectedly, the increase of tumor cell radiosensitivity, α, has a positive effect on treatment efficacy, leading to the monotonic decrease of the minimal number of alive tumor cells during radiotherapy. Variation of tumor cell proliferation rate, B, however, has an ambiguous effect. For relatively radioresistant tumors, the increase of B decreases the treatment efficacy, since tumor cell repopulation acts as a major obstacle for tumor cure, compensating for cell killing. For radiosensitive tumors, however, treatment efficacy depends on B in non-linear fashion. As B increases from 0.01 to 0.04, initially the number of tumor cells after radiotherapy declines. This happens due to the fact that for an efficient treatment fast transition of tumor cells from quiescent to proliferative state represents a positive feature, since it renders the tumor cells more radiosensitive and thus easier to kill. Nevertheless, under further increase of B tumor cell repopulation significantly hinders the radiotherapy efficacy as well.

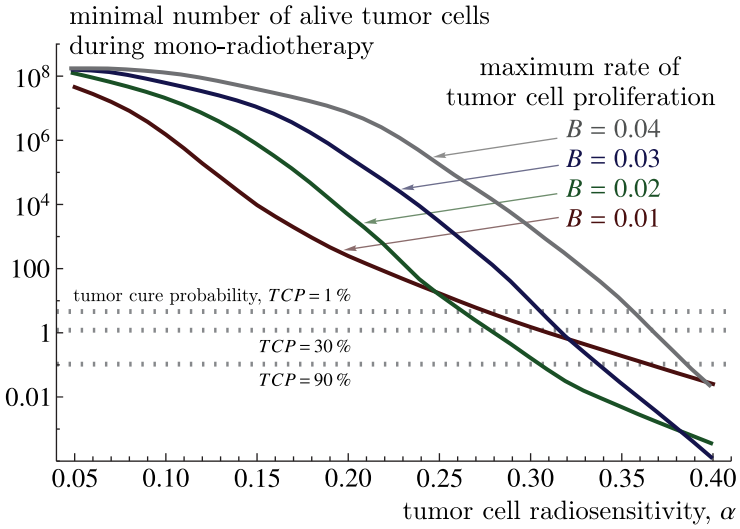

Figure 3. Minimal number of alive tumor cells during radiotherapy without the use of radiosensitizing nanoparticles and without antiangiogenic therapy during model simulations under variation of tumor cell radiosensitivity, α, and maximum tumor cell proliferation rate, B

Search for optimized protocols for proton radiotherapy with nanosensitizers and antiangiogenic therapy

For the same variation of parameters, depicted in Fig. 3, we further compared the efficacy of several types of combined treatments. The first type is radiotherapy combined with antiangiogenic

therapy, starting simultaneously. The second type of treatment is radiotherapy with the use of radiosensitizing nanoparticles, injected two days before the first irradiations of each of the first n weeks, where $n = 1, \ldots, 6$. The third type of treatment involves radiotherapy with nanosentitizers and antiangiogenic therapy, starting along with the irradiation following the last nanoparticles injection. We did not consider antiangiogenic therapy starting before the last nanoparticles injection, as it would mitigate their inflow in tumor.

Figure 4 illustrates the outcome of comparison of these treatments, in terms of the relative minimal number of alive tumor cells, compared to mono-radiotherapy. For slowly growing and relatively radiosensitive tumors ($B = 0.1$, $\alpha > 0.09$) the addition of antiangiogenic therapy to radiotherapy turns out to be detrimental, increasing the minimal number of alive tumor cells up to ≈ 2.2-fold, as Fig. 4, *a* shows. This aligns with our previous findings [Kuznetsov et al., 2018] and is explained by the fact that tumors subject to antiangiogenic therapy receive less oxygen and nutrients and thus effectively remain less radiosensitive. For faster proliferating tumors ($B \geqslant 0.2$), however, addition of antiangiogenic therapy to radiotherapy allows reducing tumor growth significantly enough to become beneficial, as Figs. 4, *b*, *c*, *d* demonstrate.

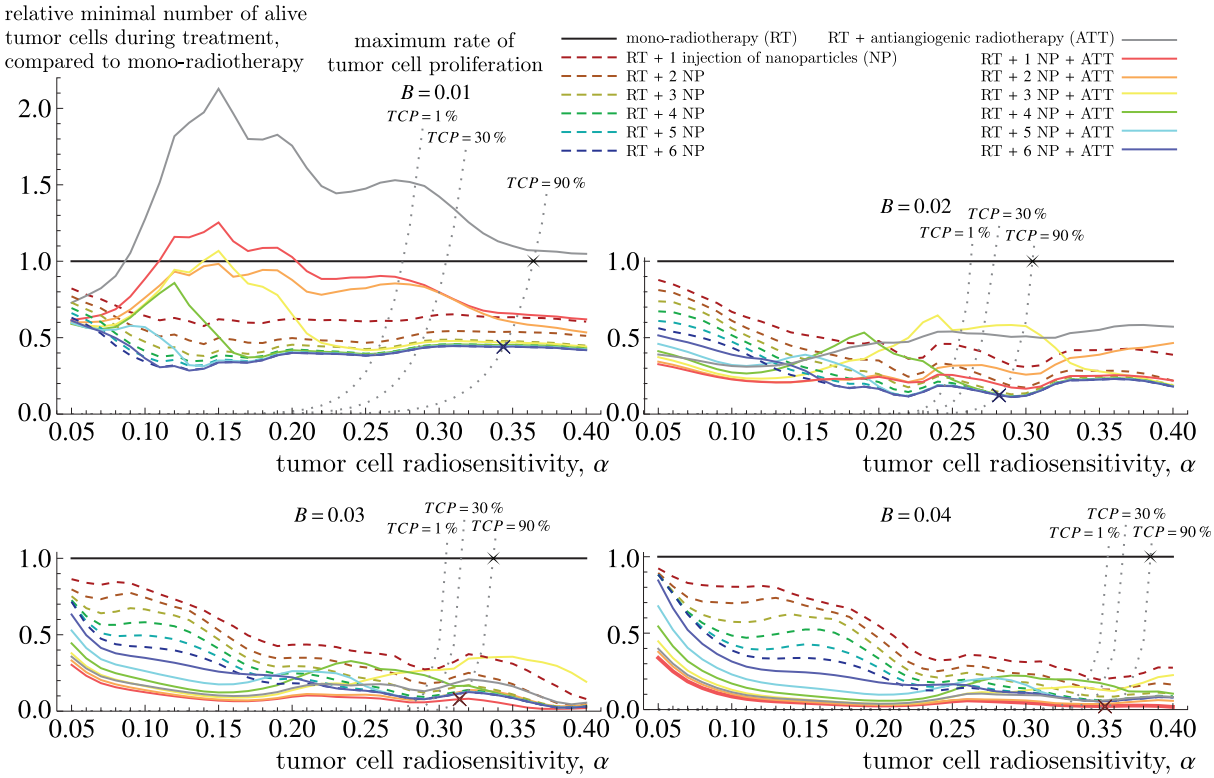

Figure 4. Relative minimal number of alive tumor cells with respect to mono-radiotherapy simulations, depicted in Fig. 3, during different types of treatments: mono-radiotherapy (yielding unity, black lines), radiotherapy with antiangiogenic therapy (gray lines), and radiotherapy with the use of radiosensitizing nanoparticles with antiangiogenic therapy (solid lines) and without antiangiogenic therapy (dashed lines), during model simulations under variation of tumor cell radiosensitivity, α, and maximum tumor cell proliferation rate, B. Radiotherapy involves 30 irradiations administered on weekdays over six consecutive weeks (implied to start on Monday). Injections of nanoparticles are performed two days before the first irradiations of each of the first n weeks (on Saturdays), where $n = 1, \ldots, 6$. Antiangiogenic therapy starts along with the irradiation following the last nanoparticles injection (on one of Mondays), or in the absence thereof — along with the first irradiation. The gray dotted lines are isocurves corresponding to fixed values of tumor cure probability (TCP), their intersections with lines corresponding to mono-radiotherapy and optimal treatments are marked with crosses

The use of nanosensitizers along with radiotherapy is beneficial for all the parameter sets considered, while the increase in the number of injections of nanoparticles results in a monotonic increase of treatment efficacy, being more prominent for relatively radiosensitive tumors.

In contrast, addition of antiangiogenic therapy to radiotherapy with nanosensitizers has an ambiguous effect. As Fig. 4, *a* shows, under tumor cell proliferation rate $B = 0.1$ for such combined treatment the start of antiangiogenic therapy after six injections of nanoparticles represents the best option for almost all values of α. However, this treatment shows similar efficiency to radiotherapy with six nanoparticle injections without antiangiogenic therapy, meaning that its addition does not enhance treatment efficacy. As tumor cell proliferation rate grows, the optimal treatment changes to radiotherapy with one injection of nanoparticles and antiangiogenic therapy starting after it. This type of treatment turns out to be more beneficial for relatively radioresistant tumors ($\alpha < 0.16$) with $B = 0.02$, as Fig. 4, *b* shows, and for all examined values of α for fast-growing tumors with $B = 0.03$ and $B = 0.04$, as Figs. 4, *c*, *d* show.

Overall, the modeling results suggest that the addition of antiangiogenic therapy to proton therapy, both with and without the use of radiosensitizing nanoparticles, is beneficial for relatively rapidly growing tumors and radioresistant tumors with moderate growth rate. For them, administration of proton therapy with one preliminary injection of nanosensitizers followed by antiangiogenic therapy represent the most efficient of the considered options. For slowly growing tumors, radiotherapy with the maximum number of injections of nanosensitizers without antiangiogenic therapy is a more efficient option, with enhancement of treatment efficacy growing with the increase of tumor radiosensitivity. However, the modeling results also suggest that the range of potentially curable tumors can increase only moderately due to the use of nanosensitizers and antiangiogenic drugs. For example, at every examined value of B, the range of tumor cell radiosensitivity values α for which $TCP = 90\,\%$ can be achieved increases by only 0.02–0.03 for optimal treatments compared to mono-radiotherapy.

Discussion

Considering the widespread use of radiotherapy and its applicability to the majority of tumors, optimizing radiotherapy presents an efficient approach to increasing the overall cancer cure rate [Joiner, van der Kogel, 2018]. Combined use of proton therapy with radiosensitizing nanoparticles and antiangiogenic therapy is a promising option towards the increase of treatment efficacy. This modeling study proposes that the optimal method of combining these modalities should crucially depend on proliferation rate and inherent radiosensitivity of tumor cells. For rapidly proliferating tumors, faster suppression of angiogenesis represents an efficient way towards minimization of tumor cell repopulation, facilitating tumor cell killing by irradiation. For slowly proliferating tumors maximization of tumor cells exposure to nanosensitizers is the most optimal approach, while the addition of antiangiogenic therapy should not contribute to faster elimination of tumor cells.

However, given the experimentally estimated increase in irradiation efficiency offered by nanosensitizers, this study suggests that their overall contribution to enhancing treatment efficacy may be only relatively modest. More studies are needed to optimize nanoparticles design in order to increase their radiosensitization properties and to improve tumor targeting and uptake. A major obstacle for intratumoral penetration of nanoparticles during prolonged radiation treatment should be the normalization of tumor-associated microvasculature. After elimination of a significant fraction of tumor cells, it should happen even in the absence of antiangiogenic therapy. Reduced competition of tumor cells for nutrients would lead to increased nutrient levels inside the tumor alleviating nutrient deficiency of tumor cells, which is required for their continuous secretion of proangiogenic factors. Enhancement of capillary permeability and therefore intratumoral delivery of nanoparticles via focused ultrasound represents an intriguing option to overcome this issue. Nowadays, this technique is employed

predominantly for disruption of blood-brain barrier, however, there are no technical limitations for implementing in for tumor sites other than brain [López-Aguirre et al., 2024].

One aspect not accounted for in the presented model is host immune response to radiotherapy. Generally, greater tumor cell kill due to the nanosensitizers effect should promote faster release of tumor-associated neoantigens, yielding increased antitumor immune response [Mellman et al., 2023]. This effect may provide additional boost of the efficacy of proton therapy utilizing nanosensitizers. However, stimulation of immune response during radiotherapy is difficult to predict, while its strength can vary dramatically, especially given that in many cancer patients the immune system is already compromised [Cheng et al., 2020]. The immune response to radiotherapy is additionally complicated by the fact that radiotherapy can also have immunosuppressive effects [Wang et al., 2024].

Another technique that can contribute to further increase of efficacy of radiotherapy with nanosensitizers is spatial and temporal optimization of irradiation. As our previous studies suggest, alteration of radiotherapy fractionation bears significant potential, especially for large tumors with prominent necrotic areas [Kuznetsov, Kolobov, 2023b; Kuznetsov, Kolobov, 2022]. Intriguingly, recent clinical results confirm the potential of dose-painting approach, accentuating proliferative and therefore radiosensitive tumor areas during radiotherapy, highlighting the need for further relevant studies [Berwouts et al., 2017].

References

Androjna C., Gatica J. E., Belovich J. M., Derwin K. A. Oxygen diffusion through natural extracellular matrices: implications for estimating “critical thickness” values in tendon tissue engineering // Comparative biochemistry and physiology part A: Physiology. — 2008. — Vol. 14, No. 4. — P. 559–569.

Azarkin M., Kirakosyan M., Ryabov V. Study of nuclear reactions in therapy of tumors with proton beams // International Journal of Molecular Sciences. — 2023. — Vol. 24, No. 174. — P. 13400.

Baker P. G. B., Mottram R. F. Metabolism of exercising and resting human skeletal muscle, in the post-prandial and fasting states // Clinical science. — 1973. — Vol. 44, No. 5. — P. 479–491.

Bendavid J., Modesto A. Radiation therapy and antiangiogenic therapy: Opportunities and challenges // Cancer/Radiothérapie. — 2022. — Vol. 26, No. 6–7. — P. 962–967.

Berwouts D., Madani I., Duprez F., Olteanu A. L., Vercauteren T., Boterberg T., Deron P., Bonte K., Huvenne W., De Neve W., Goethals I. Long-term outcome of 18F-fluorodeoxyglucose-positron emission tomography-guided dose painting for head and neck cancer: matched case-control study // Head & Neck. — 2017. — Vol. 39, No. 11. — P. 2264–2275.

Bilynsky C., Millot N., Papa A. Radiation nanosensitizers in cancer therapy—From preclinical discoveries to the outcomes of early clinical trials // Bioengineering & Translational Medicine. — 2022. — Vol. 7, No. 1. — P. e10256.

Brown A., Suit H. The centenary of the discovery of the Bragg peak // Radiotherapy and oncology. — 2004. — Vol. 73, No. 3. — P. 265–268.

Casciari J. J., Sotirchos S. V., Sutherland R. M. Mathematical modelling of microenvironment and growth in EMT6/Ro multicellular tumour spheroids // Cell proliferation. — 1992. — Vol. 25, No. 1. — P. 1–22.

Cheng S., Cheadle J. E., Illidge M. T. Understanding the effects of radiotherapy on the tumour immune microenvironment to identify potential prognostic and predictive biomarkers of radiotherapy response // Cancers. — 2020. — Vol. 12, No. 10. — P. 2835.

Chuang Y. C., Wu P. H., Shen Y. A., Kuo C. C., Wang W. J., Chen Y. C., Lee H. L., Chiou J. F. Recent advances in metal-based nanoenhancers for particle therapy // Nanomaterials. — 2023. — Vol. 13, No. 6. — P. 1011.

Clerbaux T., Gustin P., Detry B., Cao M. L., Frans A. Comparative study of the oxyhaemoglobin dissociation curve of four mammals: man, dog, horse and cattle // Comparative biochemistry and physiology part A: Physiology. — 1993. — Vol. 106, No. 4. — P. 687–694.

Clough G., Smaje L. H. Exchange area and surface properties of the microvasculature of the rabbit submandibular gland following duct ligation // The journal of physiology. — 1984. — Vol. 354, No. 1. — P. 445–456.

Cunningham C., de Kock M., Engelbrecht M., Miles X., Slabbert J., Vandevoorde C. Radiosensitization effect of gold nanoparticles in proton therapy // Frontiers in Public Health. — 2021. — Vol. 9. — P. 699822.

Dickson P. V., Hamner J. B., Sims T. L., Fraga C. H., Ng C. Y. C., Rajasekeran S., Hagedorn N. L., McCarville M. B., Stewart C. F., Davidoff A. M. Bevacizumab-induced transient remodeling of the vasculature in neuroblastoma xenografts results in improved delivery and efficacy of systemically administered chemotherapy // Clinical cancer research. — 2007. — Vol. 13, No. 13. — P. 3942–3950.

Dings R. P. M., Loren M., Heun H., McNiel E., Griffioen A. W., Mayo K. H., Griffin R. J. Scheduling of radiation with angiogenesis inhibitors Anginex and Avastin improves therapeutic outcome via vessel normalization // Clinical cancer research. — 2007. — Vol. 13, No. 11. — P. 3395–3402.

Freyer J., Sutherland R. A reduction in the in situ rates of oxygen and glucose consumption of cells in EMT6/Ro spheroids during growth // J. Cell Physiol. — 1985. — Vol. 124, No. 3. — P. 516–524.

Galanakou P., Theodora L., Wazir M. Non-radioactive elements for prompt gamma enhancement in proton therapy // Radiation Physics and Chemistry. — 2022. — Vol. 196 — P. 110132.

Gee M., Procopio W. N., Makonnen S., Feldman M. D., Yeilding N. M., Lee W. M. Tumor vessel development and maturation impose limits on the effectiveness of anti-vascular therapy // The American journal of pathology. — 2003. — Vol. 162, No. 1. — P. 183–193.

Goedegebuure R., De Klerk L. K., Bass A. J., Derks S., Thijssen V. L. Combining radiotherapy with anti-angiogenic therapy and immunotherapy; a therapeutic triad for cancer? // Frontiers in immunology. — 2019. — Vol. 9. — P. 3107.

Hanahan D., Weinberg R. The hallmarks of cancer // Cell. — 2000. — Vol. 100, No. 1. — P. 57–70.

Holash J. M. P. C., Maisonpierre P. C., Compton D., Boland P., Alexander C. R., Zagzag D., Yancopoulos G. D., Wiegand S. J. Vessel cooption, regression, and growth in tumors mediated by angiopoietins and VEGF // Science. — 1999. — Vol. 284. — P. 1994–1998.

Hu X., Hu J., Pang Y., Wang M., Zhou W., Xie X., Zhu C., Wang X., Sun X. Application of nano-radiosensitizers in non-small cell lung cancer // Frontiers in Oncology. — 2024. — Vol. 14. — P. 1372780.

Hu Y., Paris S., Sahoo N., Bertolet G., Wang Q., Wang Q., Barsoumian H. B., Da Silva J., Huang A., Doss D. J., Pollock D. P., Hsu E., Selene N., Kettlun Leyton C. S., Voss T. A., Masrorpour F., Ganjoo S., Leuschner C., Pietz J. T., Puebla-Osorio N., Gandhi S., Nguyen Q.-N., Wang J., Cortez M. A., Welsh J. W. Nanoparticle-enhanced proton beam immunoradiotherapy drives immune activation and durable tumor rejection // JCI insight. — 2023. — Vol. 8, No. 12.

Iwata H., Ogino H., Hashimoto S., Yamada M., Shibata H., Yasui K., Toshito T., Omachi C., Tatekawa K., Manabe Y., Mizoe J., Shibamoto Y. Spot scanning and passive scattering proton therapy: Relative biological effectiveness and oxygen enhancement ratio in cultured cells // International journal of radiation oncology · biology · physics. — 2016. — Vol. 95, No. 1. — P. 95–102.

Jain R. Normalization of tumor vasculature: an emerging concept in antiangiogenic therapy // Science — 2005. — Vol. 307, No. 5706. — P. 58–62.

Jayson J., Kerbel R., Ellis L. M., Harris A. L. Antiangiogenic therapy in oncology: current status and future directions // The Lancet. — 2016. — Vol. 388, No. 10043. — P. 518–529.

Joiner M. C., van der Kogel A. J. Basic clinical radiobiology. — CRC press, 2018.

Köhn-Luque A., De Back W., Yamaguchi Y., Yoshimura K., Herrero M. A., Miura T. Dynamics of VEGF matrix-retention in vascular network patterning // Physical biology. — 2013. — Vol. 10, No. 6. — P. 066007.

Kelm J. M., Sanchez-Bustamante C. D., Ehler E., Hoerstrup S. P., Djonov V., Ittner L., Fussenegger M. VEGF profiling and angiogenesis in human microtissues // Journal of biotechnology. — 2005. — Vol. 118, No. 2. — P. 213–229.

Kuznetsov M., Gubernov V., Kolobov A. Analysis of anticancer efficiency of combined fractionated radiotherapy and antiangiogenic therapy via mathematical modelling // Russian Journal of Numerical Analysis and Mathematical Modelling. — 2018. — Vol. 33, No. 4. — P. 225–242.

Kuznetsov M., Kolobov A. Mathematical modelling for spatial optimization of irradiation during proton radiotherapy with nanosensitizers // Russian Journal of Numerical Analysis and Mathematical Modelling. — 2023a. — Vol. 38, No. 5. — P. 303–321.

Kuznetsov M., Kolobov A. Optimization of antitumor radiotherapy fractionation via mathematical modeling with account of 4 R's of radiobiology // Journal of Theoretical Biology. — 2023b. — Vol. 558. — P. 111371.

Kuznetsov M., Kolobov A. Optimization of dose fractionation for radiotherapy of a solid tumor with account of oxygen effect and proliferative heterogeneity // Mathematics. — 2020. — Vol. 8, No. 8. — P. 1204.

Kuznetsov M., Kolobov A. Optimization of size of nanosensitizers for antitumor radiotherapy using mathematical modeling // International Journal of Molecular Sciences. — 2023c. — Vol. 24, No. 14. — P. 11806.

Kuznetsov M., Kolobov A. Spatial optimization of fractionated proton therapy via mathematical modeling // Bulletin of the Lebedev Physics Institute. — 2022. — Vol. 49, No. 6. — P. 174–179.

Kuznetsov M., Kolobov A. Transient alleviation of tumor hypoxia during first days of antiangiogenic therapy as a result of therapy-induced alterations in nutrient supply and tumor metabolism–Analysis by mathematical modeling // Journal of theoretical biology. — 2018. — Vol. 451. — P. 86–100.

Leder K., Pitter K., LaPlant Q., Hambardzumyan D., Ross B. D., Chan T. A., Holland E. C., Michor F. Mathematical modeling of PDGF-driven glioblastoma reveals optimized radiation dosing schedules // Cell. — 2014. — Vol. 156, No. 3. — P. 603–616.

López A., Parsai S., Joshi N., Godley A., Shah C., Koyfman S.A., Caudell J. J., Fuller C. D., Enderling H., Scott J. G. Temporally feathered intensity-modulated radiation therapy: A planning technique to reduce normal tissue toxicity // Medical physics. — 2018. — Vol. 45, No. 7. — P. 603–616, 3466–3474.

López-Aguirre M., Castillo-Ortiz M., Viña-González A., Blesa J., Pineda-Pardo J. A. The road ahead to successful BBB opening and drug-delivery with focused ultrasound // Journal of Controlled Release. — 2024. — Vol. 372. — P. 901–913.

Mac Gabhann F., Popel A. S. Interactions of VEGF isoforms with VEGFR-1, VEGFR-2, and neuropilin in vivo: a computational model of human skeletal muscle // American journal of physiology – Heart and circulatory physiology. — 2007. — Vol. 292, No. 1. — P. H459–H474.

McDonald T., Cheng Y. C., Graser C., Nicol P. B., Temko D., Michor F. Computational approaches to modelling and optimizing cancer treatment // Nature Reviews Bioengineering. — 2023. — Vol. 1, No. 10. — P. 695–711.

Mellman I., Chen D. S., Powles T., Turley S. J. The cancer-immunity cycle: Indication, genotype, and immunotype // Immunity. — 2023. — Vol. 56, No. 10. — P. 2188–2205.

Munro T., Gilbert C. The relation between tumour lethal doses and the radiosensitivity of tumour cells // The British journal of radiology. — 1961. — Vol. 34, No. 400. — P. 246–251.

Patra K., Hay N. The pentose phosphate pathway and cancer // Trends in biochemical sciences. — 2014. — Vol. 39, No. 8. — P. 347–354.

Pittman R. N., van der Kogel A. J. Regulation of tissue oxygenation // Colloquium series on integrated systems physiology: from molecule to function. — Morgan & Claypool Life Sciences, 2011.

Popov A., Kolmanovich D., Chukavin N., Zelepukin I., Tikhonowski G., Pastukhov A., Popov A., Shemyakov A., Klimentov S., Ryabov V., Deyev S., Zavestovskaya I., Kabashin A. Boron nanoparticle-enhanced proton therapy: molecular mechanisms of tumor cell sensitization // Molecules. — 2024. — Vol. 29, No. 16. — P. 3936.

Press W. H. Numerical recipes: The art of scientific computing. — 3rd ed. — Cambridge university press, 2007.

Prokopiou S., Moros E. G., Poleszczuk J., Caudell J., Torres-Roca J. F., Latifi K., Lee J. K., Myerson R., Harrison L. B., Enderling H. A proliferation saturation index to predict radiation response and personalize radiotherapy fractionation // Radiation Oncology. — 2015. — Vol. 10. — P. 1–8.

Richardson R. S., Duteil S., Wary C., Wray D. W., Hoff J., Carlier P. G. Human skeletal muscle intracellular oxygenation: the impact of ambient oxygen availability // The journal of physiology. — 2006. — Vol. 571, No. 2. — P. 415–424.

Song X., Sun Z., Li L., Zhou L., Yuan S. Application of nanomedicine in radiotherapy sensitization // Frontiers in Oncology. — 2023. — Vol. 13. — P. 1088878.

Stamatelos S. K., Kim E., Pathak A. P., Popel A. S. A bioimage informatics based reconstruction of breast tumor microvasculature with computational blood flow predictions // Microvascular research. — 2014. — Vol. 91. — P. 8–21.

Tsang D., Timmerman B. Improving access to proton therapy in the United States and around the world // International Journal of Radiation Oncology, Biology, Physics. — 2004. — Vol. 119, No. 4. — P. 1078–1081.

Tuchin V. V., Bashkatov A. N., Genina E. A., Sinichkin Y. P., Lakodina N. A. In vivo investigation of the immersion-liquid-induced human skin clearing dynamics // Technical physics letters. — 2001. — Vol. 27, No. 6. — P. 489–490.

Wang L., Lynch C., Pitroda S. P., Piffkó A., Yang K., Huser A. K., Liang H. L., Weichselbaum R. R. Radiotherapy and immunology // Journal of Experimental Medicine. — 2024. — Vol. 221, No. 7. — P. e20232101.

Wouters B. G., Brown J. M. Cells at intermediate oxygen levels can be more important than the “hypoxic fraction” in determining tumor response to fractionated radiotherapy // Radiation research. — 1997. — Vol. 147, No. 5. — P. 541–550.

Wu J. The enhanced permeability and retention (EPR) effect: The significance of the concept and methods to enhance its application // Journal of personalized medicine. — 2021. — Vol. 11, No. 8. — P. 771.

Zavestovskaya I., Popov A., Kolmanovich D., Tikhonowski G., Pastukhov A., Savinov M., Shakhov P., Babkova J., Popov A., Zelepukin I., Grigoryeva M., Shemyakov A., Klimentov S., Ryabov V., Prasad P., Deyev S., Kabashin A. Boron nanoparticle-enhanced proton therapy for cancer treatment // Nanomaterials. — 2023. — Vol. 13, No. 15. — P. 2167.

Zavestovskaya I., Filimonova M., Popov A., Zelepukin I., Shemyakov A., Tikhonowski G., Savinov M., Filimonov A., Shitova A., Soldatova O., Kolmanovich D., Shakhov P., Kotelnikova P., Popov A.,

Chukavin N., Pivovarov N., Syuy A., Klimentov S., Ryabov V., Ivanov S., Kaprin A., Prasad P., Deyev S., Koryakin S., Kabashin A. Bismuth nanoparticles-enhanced proton therapy: Concept and biological assessment // Materials Today Nano. — 2024. — Vol. 27. — P. 100508.

Zelepukin I., Yaremenko A., Petersen E., Deyev S., Cherkasov V., Nikitin P., Nikitin M. Magnetometry based method for investigation of nanoparticle clearance from circulation in a liver perfusion model // Nanotechnology. — 2019. — Vol. 30, No. 10. — P. 105101.

Zhao L., Wu D., Mi D., Sun Y. Radiosensitivity and relative biological effectiveness based on a generalized target model // Journal of radiation research. — 2017. — Vol. 58, No. 1. — P. 8–16.